Journal of Power Sources 195 (2010) 6024–6030

Contents lists available at ScienceDirect

Journal of Power Sources

journal homepage: www.elsevier.com/locate/jpowsour

Study on the dynamic behavior of Zn-based hydrogen generating cells as fuel storage for a PEM micro fuel cell system

M. Weiland[a,*], S. Krumbholz[a], S. Wagner[b], H. Reichl[a]

[a] Technische Universität Berlin, Center of Microperipherics, Gustav-Meyer-Allee 25, 13355 Berlin, Germany
[b] Fraunhofer Institute for Reliability and Microintegration, 13355 Berlin, Germany

ARTICLE INFO

Article history:
Received 2 October 2009
Received in revised form
13 November 2009
Accepted 16 November 2009
Available online 20 November 2009

Keywords:
Micro fuel cell system
Hydrogen generation "on demand"
Transient voltage
Current interrupt

ABSTRACT

Portable fuel cell systems consist of three essential parts: the fuel cell stack, the fuel storage and the balance of plant (BOP) which contains all required peripheral components. Scaling down fuel cell systems to smaller dimensions in the power range of 1 mW to 1 W currently leads to an increased volume fraction of the peripheral components. Consequently it is necessary to forego peripheral components in small systems and develop passive systems. Furthermore fuel storage is a challenging issue for portable micro fuel cell systems. Common approaches for hydrogen storage, e.g. pressure cartridges or reversible metal hydrides yield a low energy density for the entire system. In our approach a gas evolving cell (GEC) is used to generate hydrogen "on demand". This allows to develop small micro fuel cell systems with a high energy density. The GEC is electrically connected in series to the fuel cell. Hydrogen is generated through the electro catalytic Zn-H_2O reaction and proportional to the cell current according to Faraday's law, which leads to a simple and passive system.

The dynamic and long-term behavior of the GEC is studied experimentally in this work. The electrical and chemical behavior of the GEC plays an important role in the design and operation of the micro fuel cell system. Portable applications generally imply dynamic load profiles. Therefore the study focuses on the dynamic response of the GEC. The electric response of the GEC is examined for load pulses in the range of milliseconds with an amplitude of up to 150 mA for the lifecycle of a cell. The results are compared to the behavior of the GECs under an equivalent static load in order to draw conclusions on the effect of the dynamic load. Furthermore the electrical and chemical capacity of the GECs is examined for different loads.

The obtained results provide an insight into the dynamic behavior of the GEC and provide the basis for the design and operation of the micro fuel cell system.

1. Introduction

The ongoing miniaturisation of electronic devices leads to an increasing spread of self-contained portable and highly integrated small size applications. Related to this there is a strong need for new concepts to power these portable applications. Because of the direct conversion from chemical energy to electric energy fuel cells are a promising approach and have achieved a broad attention during the last couple of years. Portable fuel cell systems consist of three essential parts: the fuel cell stack itself, the fuel storage and the balance of plant (BOP) which contains all required peripheral components. When scaling down fuel cell systems to smaller dimensions in the power range of 1 mW to 1 W, currently the volume fraction of peripheral components is strongly increased. This results in a demand for passive systems. The development and optimization of our self-breathing passive micro fuel cells is discussed in [1–4]. Another key issue for portable systems however is the fuel storage. Common approaches like gaseous storage in pressure cartridges and reversible metal hydrides implicate high weights which in turn lead to a smaller energy density for the entire system [5]. The approach to store hydrogen chemically usually leads to an increased BOP due to the need of additional components like reformers, pumps and reactors. In our approach a gas evolving cell (GEC) is used to generate hydrogen "on demand" through the electro catalytic Zn-H_2O reaction. The generated hydrogen is proportional to the GEC current according to Faraday's law. Connecting the GEC in series to a micro fuel cell thus leads to a simple and passive system, with no need for any valves or pressure controllers. In principle the energy density of zinc-air batteries can be achieved with this system. In contrast to usual zinc-air batteries however environmental driven degradation [6,7] is prevented as the cathode of the GEC is directly connected to the anode of the

* Corresponding author. Tel.: +49 30 46403 728; fax: +49 30 46403 123.
E-mail address: matthias.weiland@becap.tu-berlin.de (M. Weiland).

0378-7753/$ – see front matter © 2009 Elsevier B.V. All rights reserved.
doi:10.1016/j.jpowsour.2009.11.063

Nomenclature

L_{dl}	thickness of the double layer [m]
a	specific area [m^{-1}]
C	double layer capacitance [$F\,m^{-2}$]
κ	ionic conductivity [$S\,m^{-1}$]
σ	electronic conductivity [$S\,m^{-1}$]
L_D	diffusion length/boundary-layer thickness [m]
D	diffusion coefficient [$m^2\,s^{-1}$]
R	universal gas constant [$Pa\,m^3\,mol^{-1}\,K^{-1}$]
T	temperature [K]
P	pressure [Pa]
F	Faraday constant [$C\,mol^{-1}$]
C_{H_2}	hydrogen concentration [$mol\,m^{-3}$]
A	cross-sectional area of the pneumatic tray [m^2]
τ	time constant dynamic response [s]

micro fuel cell and thus separated from the environment, which yields a higher long time stability. Although not intended at the moment, the cells theoretically can be recharged mechanically by replacing the anode.

2. Theory

2.1. Concept of the GEC

In principle the studied GEC is a modified button type zinc-air battery. According to the manufacturer VARTA Microbattery GmbH the gas generating cathode of the cell is modified and optimized for hydrogen generation. The general structure of the GEC is illustrated in Fig. 1. The GEC volume is approximately 3 cm^3. Similar to a typical zinc-air battery the zinc anode is consisting of zinc granules and the aqueous electrolyte is stored in the anode can, which is insulated from the cathode by a separator and a plastic gasket. On the cathode side a metallic mesh is coated with Raney nickel, which is used as the catalyst. An additional hydrogen permeable PTFE-layer is used as a gasket. Furthermore the GEC is sealed off with an adhesive tape at the hydrogen outlet in order to prevent oxygen from getting into the cathode compartment when stored.

The discharge reaction of the typical zinc-air battery can be stated as [6]:

$$\begin{aligned} &\text{zinc oxidation (anode)}: 2Zn + 4OH^- \rightarrow 2ZnO + 2H_2O + 4e^- \\ &\text{oxygen reduction (cathode)}: \quad 2H_2O + O_2 + 4e^- \rightarrow 4OH^- \\ &\text{overall reaction}: 2Zn + O_2 \rightarrow 2ZnO \end{aligned} \tag{1}$$

By suppressing the oxygen supply on the cathode side of the GEC the reactions are changed to:

$$\begin{aligned} &\text{zinc oxidation (anode)}: 2Zn + 4OH^- \rightarrow 2ZnO + 2H_2O + 4e^- \\ &\text{water reduction (cathode)}: 4H_2O + 4e^- \rightarrow 2H_2O + 4OH^- \\ &\text{overall reaction}: 2Zn + 2H_2O \rightarrow 2ZnO + 2H_2 \end{aligned} \tag{2}$$

Resulting from the overall reactions in above Eqs. (1) and (2) a decrease of the resulting change in Gibbs free energy can be observed. This leads to a drop of the nominal cell voltage of the GEC from 1.65 V down to 0.42 V assuming standard conditions.

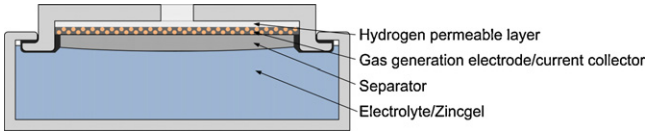

Fig. 1. Schematic of the general structure of the GEC.

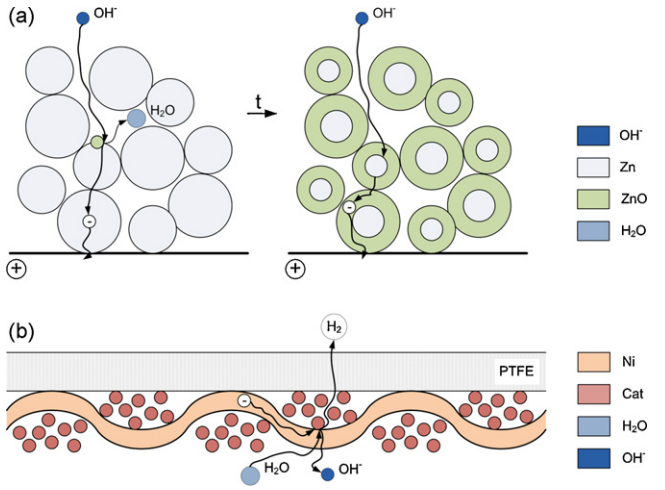

Fig. 2. Schematic of the reactions of the GEC: (a) anode and (b) cathode.

The cell reactions for the GEC are illustrated in Fig. 2. As illustrated solely the anode of the cell is consumed during discharge. With increasing discharge time the fraction of ZnO is increasing within the anode volume, whereas the fraction of Zn is decreased. This might yield a change of the mean ionic and electric conductivities leading to a change of the total impedance of the cell.

2.2. Dynamic characteristics of the GEC

In addition to the need for high energy densities in portable applications, the dynamic behavior of the power supply plays an important role. Due to the self-contained design portable applications generally imply dynamic load profiles. There is a specific time period where the system is in stand-by and hardly consumes any power followed by a short period of activity where for example data is gathered and transmitted in sensor-nodes. Therefore this study focuses on the dynamic response of the GEC. Due to the complexity of the electrochemical system several dynamic effects are superposed in the GEC.

One effect leading to a dynamic response of electrochemical systems is the double layer charging effect. It originates from charge separation at the two electrodes where ions and electrons are separated. While the ions are transferred to the other electrode through the electrolyte, the electrons are blocked by the electrolyte and have to pass through an external load. Two layers of opposite charge are formed at the boundary of each electrode. In an electric circuit model this can be represented by a double layer capacitor in parallel to the charge transfer resistance that represents the Faradaic reaction [5,8]. The resulting time constant can be calculated [8]:

$$\tau_{dl} = {L_{dl}}^2 aC \left(\frac{1}{\kappa} + \frac{1}{\sigma}\right) \tag{3}$$

Ong and Newman [8] showed the values of 12.77 ms and 17.8 ms for the discussed lithium cell. Wang and Wang [9] estimated a value of 0.2 μs for a PEM fuel cell. The difference mainly originates in the thickness L_{dl} of the double layer, with 100 μm and 174 μm in [8] and 10 μm in [9]. As no detailed data is available for the GEC, no specific estimations can be made for the studied GEC. However a magnitude of milliseconds can be expected as the electrodes of a polymer electrolyte membrane used in fuel cells are rather thin.

Another important effect that needs to be considered when studying the dynamic behavior of electrochemical systems is mass transport. Within the passive GEC it is assumed that this is dominated by diffusion. Water needs to be transported from the anode to the cathode and hydroxide ions vice versa. Assum-

ing one-dimensional Fickian diffusion the diffusion time can be approximated [10]:

$$\tau_{\text{diff}} = \frac{{L_D}^2}{D} \tag{4}$$

However as no detailed parameters are available for the studied GEC, no estimations can be given at this point.

There are several methods to characterize the dynamic behavior of electrochemical systems, e.g. electro impedance spectroscopy and the current interrupt technique [5,6]. Although the current interrupt technique is error-prone in separating the vertical transition from the dynamic transition and an accurate identification of the parameters related to the dynamic transition is difficult, it is chosen over the electro impedance spectroscopy in this study because of the simple direct approach that allows for in situ measurements.

Mathematically the transient behavior of the cell voltage on current interrupt can be described using a series of exponential functions:

$$U_{\text{cell}} = U_0 - \sum_i^n U_i \exp\left(\frac{t_0 - t}{\tau_i}\right) \tag{5}$$

where U_0 is the open-circuit voltage, t_0 is the point time where the current is switched off, and U_i and τ_i are the amplitude and time constant of the ith exponential, respectively. If the time constant of one process is similar to the time constant of another process, the two are not distinguishable and result in the same exponential function.

3. Experiment

3.1. Experimental setup

During the experiment different GECs were discharged with a continuous and pulsed current. A Maccor Series 4000 battery test system was used as an electronic load. For the pulsed experiments a pulse width of 20 ms and rest time of 80 ms was employed, resulting in a pulse period of 100 ms and duty cycle of 0.2. As the minimum temporal resolution of the battery test system (10 ms) is not sufficient for measuring the transient response of the GEC a Keithley 2601 Source Meter together with a self-programmed LabVIEW program was employed to measure the voltage response with a resolution of 0.3 ms. However in order be able to measure with this resolution the acquisition, transfer and storage of readings had to be separated, leading to an actual measurement interval of 2 s.

The GEC was housed in an evacuated case and the outlet was let into a pneumatic tray in order to collect the generated gas and measure the hydrogen capacity of the GEC during the long-term experiments. The saturation of the water used in the pneumatic tray was ensured by leaving a certain amount of hydrogen within the tray for at least 24 h prior to every experiment. During all long-term experiments readings of the hydrogen volume within the pneumatic tray as well as environmental air pressure and water column height were taken repeatedly. All experiments were carried out at room temperature.

3.2. Measurements

First of all two GECs were discharged with continuous constant loads of 30 mA and 50 mA (the maximum continuous current specified by the manufacturer). These experiments were followed by three experiments with a pulsed load of 30 mA, 100 mA, and 150 mA. With a duty cycle of 0.2 a 150 mA pulse current is equivalent to a mean current of 30 mA. In these experiments the GECs were under load until the cell voltage dropped down to 0.0 V.

In order to characterize the dynamic response for additional currents a pulsed scan was utilized. With the same setup pulses of different amplitudes were forced onto the GEC, a sequence of 100 pulses for current levels in between 5 mA and 150 mA.

4. Experimental results and discussion

4.1. Long-term discharge experiments

The actual discharge time, electric charge and energy as well as generated hydrogen volume are given in Table 1. The measured hydrogen volume given considers ambient pressure conditions. For comparison the amount of generated hydrogen is calculated from the electric charge Q according to Faraday's law [5] and assuming an ideal gas and considering losses by diffusion through the water in the pneumatic tray ($D_{H_2} = 3.9 \times 10^{-9}\ \text{m}^2\ \text{s}^{-1}$ [11]):

$$V_{H_2,\text{calc}} = \frac{RT}{p}\frac{Q}{2F} - V_{H_2,\text{loss}} \tag{6}$$

$$V_{H_2,\text{loss}} = \frac{RT}{p} D_{H_2} \frac{C_{H_2}}{L_D} At \tag{7}$$

The calculated and measured hydrogen volumes show a very good agreement. Thus the generated volume is given as well in the table, neglecting the loss due to diffusion.

Fig. 3 shows the cell voltage over time for all long-term experiments. For each experiment with pulsed currents two curves illustrate the load level voltage and rest voltage for the entire discharge. It can be seen, that the discharge with a pulsed current at 30 mA results in the longest discharge time and most even voltage profile with a load level voltage above 0.3 V for 300 h. All other experiments show a non-uniform voltage profile.

It can be noticed that the load level voltage for the 30 mA pulsed load is not as low as the voltage level of the comparable continuous discharge at 30 mA. During the 20 ms load pulse the cell voltage does not drop down to a steady state. The electric charge and hydrogen generated during this experiment is about 13% higher compared to the comparable continuous discharge at 30 mA (Table 1). More interesting though and resulting from the voltage profile is the energy drawn from the cell, which is twice as high with 0.70 Wh in contrast to 0.34 Wh. Although the GEC is intended to be used solely for hydrogen generation together

Table 1
Summarized final values of the discharge.

I [mA]	DC [1]	I_{mean} [mA]	$t_{\text{discharge}}$ [h]	Energy [Wh]	Electric charge [Ah]	Measured hydrogen volume[a] [ml]	Calculated hydrogen volume[b] [ml]	Generated hydrogen volume[c] [ml]
30	1	30	61.97	0.34	1.86	824	827	848
50	1	50	35.26	0.26	1.76	794	793	804
30	0.2	6	336.97	0.70	2.10	832	824	956
100	0.2	20	81.88	0.33	1.58	694	696	720
150	0.2	30	56.91	0.22	1.63	724	726	742

[a] Measured using pneumatic tray and considering pressure conditions.
[b] Calculated using measured electric charge and losses due to diffusion.
[c] Calculated using pneumatic tray measurement and theoretical losses due to diffusion.

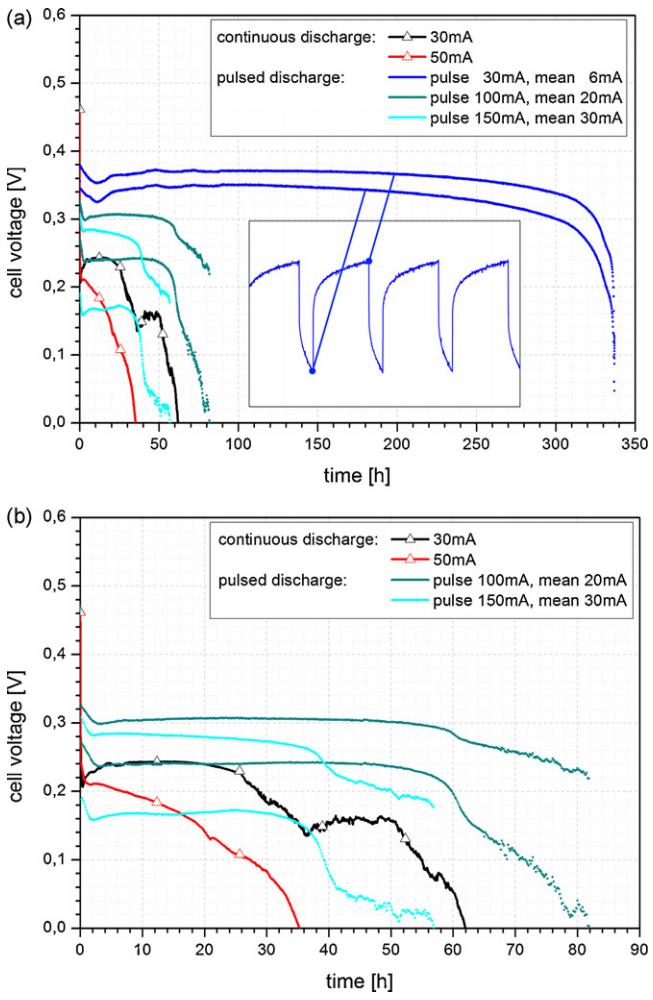

Fig. 3. Cell voltage during continuous and pulsed discharge: (a) all long-term experiments and (b) close-up of experiments with short discharge time, for comparison.

with a micro fuel cell, this should be considered for an application as the voltage level and power of the GEC add to the micro fuel cell voltage and power as both components are connected in series.

Assuming a voltage level of 0.87 V for the micro fuel cell [4] and considering a mean voltage level of 0.33 V for the GEC at 30 mA pulse load a gravimetric energy density of approximately 287 Wh kg^{-1} can be achieved neglecting the weight of the fuel cell. Compared to 252 Wh kg^{-1} with a commercially available metal hydride storage canister (Horizon FCC-020) under the same assumptions this leads to a 14% gain in energy density. It should be noted that additional pressure regulators and valves, which are necessary for the metal hydride storage, are not considered in the approximations and decrease the energy density of a system using a metal hydride storage canister even further.

Fig. 3b shows a close-up of the shorter long-term experiments. As already noted all of these experiments show a non-uniform voltage profile. The cell voltage of the continuous discharge at 30 mA shows a local minimum after 36 h, about 58% of the discharge time. Afterwards the cell voltage recovers again. The cell voltage of the continuous discharge at 50 mA shows a little dent after 21 h, as well about 58% of the discharge time. The pulsed experiments show an abrupt voltage decline after about 70% of the discharge time. It is assumed, that this behavior might be due to a change of the bulk conductivity within the GEC as described before. The pulsed discharge leads to a delay of this effect. Presumably higher currents

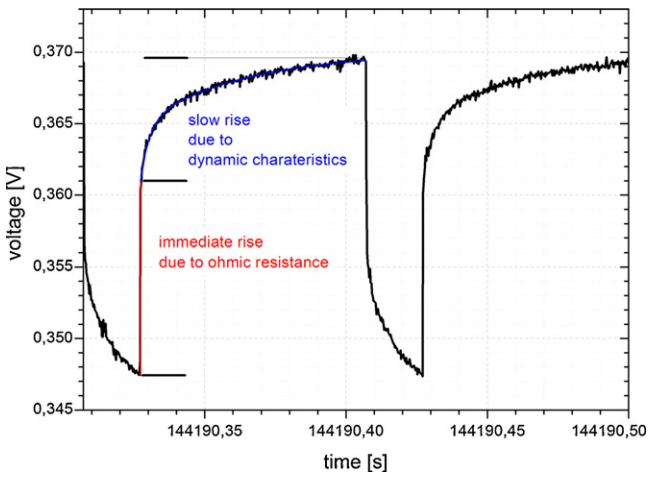

Fig. 4. Transient response to current interrupt, pulse current 30 mA.

lead to a change in the structure of the formed ZnO or a change of the cell reactions.

The principle dynamic response to the current interrupt after a load pulse is displayed in Fig. 4. As illustrated there is an immediate rise due to ohmic resistance followed by a slow rise due to the dynamic characteristics of the GEC. The data analysis software OriginLab is used to determine the parameters of the representing exponential function. Within this short current interrupt of 80 ms two superposed exponential functions can be identified. The first strong rise from 0.361 V to 0.366 V is characterized by a time constant τ_1 of 3 ms, the subsequent slow rise up to 0.369 V is characterized by a time constant τ_2 of 36 ms. Furthermore the ohmic resistance can be quantified to approximately 450 mΩ from the immediate rise.

The calculated time constants for two long-term experiments with 30 mA and 150 mA pulsed current are illustrated in Fig. 5. As both experiments lead to different discharge times, the time scale is normalized to allow comparison. It can be seen that under both load currents the GEC shows a similar transient response. The time constants calculated for the 30 mA discharge show a greater variation, which is mainly due to the smaller amplitude of the load current. Furthermore it can be noticed, that the longer time constant around 40 ms generally shows a greater variation than the shorter time constant around 3 ms. This is due to the short rest time in between subsequent pulses. Nevertheless it can be seen that the

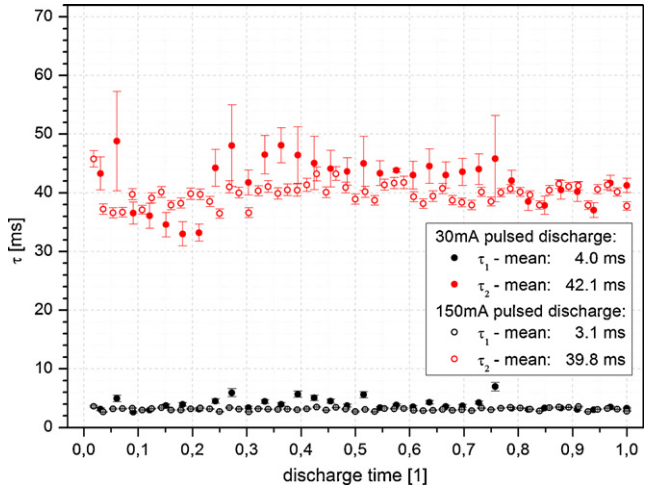

Fig. 5. Measured time constants for long time discharge, 30 mA and 150 mA pulse currents, DC = 0.2.

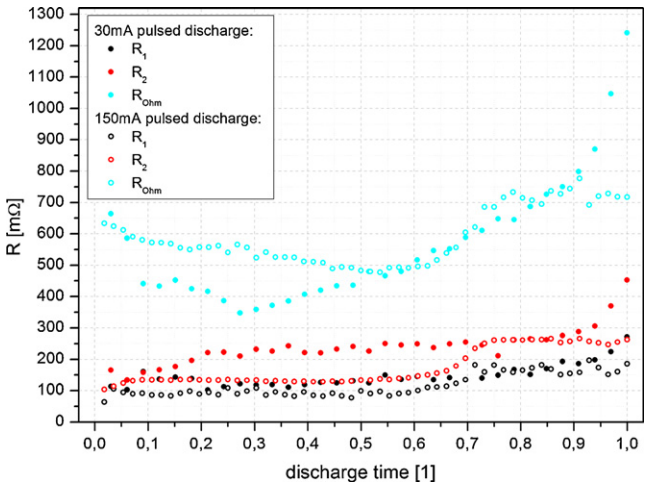

Fig. 6. Equivalent circuit resistance for long time, 30 mA and 150 mA pulse currents, DC = 0.2.

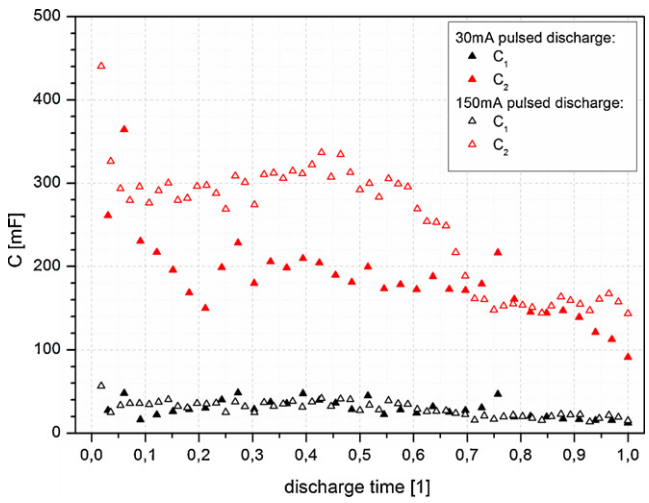

Fig. 7. Equivalent circuit capacitance from long time discharge, 30 mA and 150 mA pulse currents, DC = 0.2.

proceeding discharge of the GEC does not show an impact on any of the time constants. The mean time constants of both experiments agree fairly well with 4.0 ms and 42.1 ms for 30 mA and 3.1 ms and 39.8 ms for 150 mA.

Assuming that the dynamic response related to τ_1 and τ_2 is due to the electrochemical double layer at the cathode and anode the parameters of an equivalent electric circuit with a resistance representing the activation overvoltage (which is assumed to be almost constant at the used currents) in parallel to a capacitance representing the double layer [5] can be calculated according to Eq. (5):

$$U_i = i_{\text{cell}} R_i \tag{8}$$

$$C_i = \frac{\tau_i}{R_i} \tag{9}$$

The calculated resistances are illustrated in Fig. 6. In addition to the resistances derived from the exponential approach the ohmic resistance derived from the immediate rise of the cell voltage is shown as well in Fig. 6. The results show a broad variation as the measurement noise is amplified with the calculations. However general trends can be seen. Again the results from the experiment with the bigger amplitude show a smoother curve. At the beginning of the experiment the ohmic resistance drops down. During the experiment with the higher load current the resistance slowly decreases for about 60% of the discharge time. Then there is a significant rise after 70% of the time and the resistance remains at a high level until the end of the experiment. In contrast to the ohmic resistance R_1 and R_2 both are low at the beginning of the experiment. However both are increasing as well after about 70% of the discharge and remain on this high level until the end of the experiment. This behavior correlates to the voltage drop noted in Fig. 3b. The resistances of the lower amplitude discharge do not show this behavior, but rise continuously until the end of the experiment. This corresponds to the measured cell voltage as discussed before as well.

Fig. 7 shows the resulting equivalent capacitances. Whereas C_1 remains fairly constant during the whole experiment for both discharge currents, there is a big variation in C_2. Neglecting the big variation, which once again is attributed to the amplified error of the second exponential term, the capacitance is in the order of 300 mF at the beginning of the experiment and drops down to about 150 mF at the end of the experiment. Considering a simple parallel-plate capacitor the capacitance decreases with decreasing permittivity or surface area or increasing separation of the plates. This behavior cannot directly be transformed to the model of the electrochemical double layer which usually is described by the Helmholtz and Gouy-Chapman theories [6], but due to the changing composition of the anode an influence on the double layer behavior might be possible.

An impact of the mass transport is not considered in the long-term experiments, as it usually is assumed to be proportional to the current [6] and thus has a constant impact on the voltage response. The continuous decrease of the cell voltage within the first 2 h of the long-term measurements might be attributed to this.

4.2. Response to different amplitude of pulse currents

In order to characterize the dynamic response for additional currents another experiment was conducted using a pulsed scan. Pulses of current levels in between 5 mA and 150 mA were drawn from the GEC in a sequence of 100 each.

In addition to the dynamic behavior observed during the long-term experiments an additional relaxation was observed after each pulse sequence. Fig. 8 illustrates the calculated time constants in reference to the pulse current. The time constants derived from the current interrupt within a pulse sequence are illustrated in Fig. 8a. There is a big variation of the time constants for smaller currents which is due to the small amplitude. As the actual response to a pulse current of 5 mA was too small, the measurement was not considered in the analysis. Nevertheless it can be seen that in general the time constant is not depending on the load current. With mean magnitudes of 3.1 ms for τ_1 and 37.5 ms for τ_2 both time constants agree fairly well with the time constants derived from the measurements of the long-term experiments. The time constants observed for the current interrupt after a pulse sequence are illustrated in Fig. 8b. The calculated values originate from measurements made with the electronic load, which does not measure with a high resolution, but can be directly related to the current interrupt at the end of a sequence. Again the impact of the small amplitudes onto the calculated time constants is visible. Nevertheless it can be seen that both time constants are increasing with increasing pulse current. Assuming that this behavior is due to mass transport dominated by diffusion a boundary-layer thickness of 50 μm and 220 μm can be estimated using a diffusion coefficient of 5×10^{-9} m^2 s^{-1}.

Similar to Section 4.1 equivalent resistances and capacitances are calculated and illustrated in Figs. 9 and 10. Furthermore the ohmic resistance resulting from this experiment is shown in Fig. 9. The calculated ohmic resistance seems to be bigger at smaller currents. In general it is assumed that the electronic load manages to

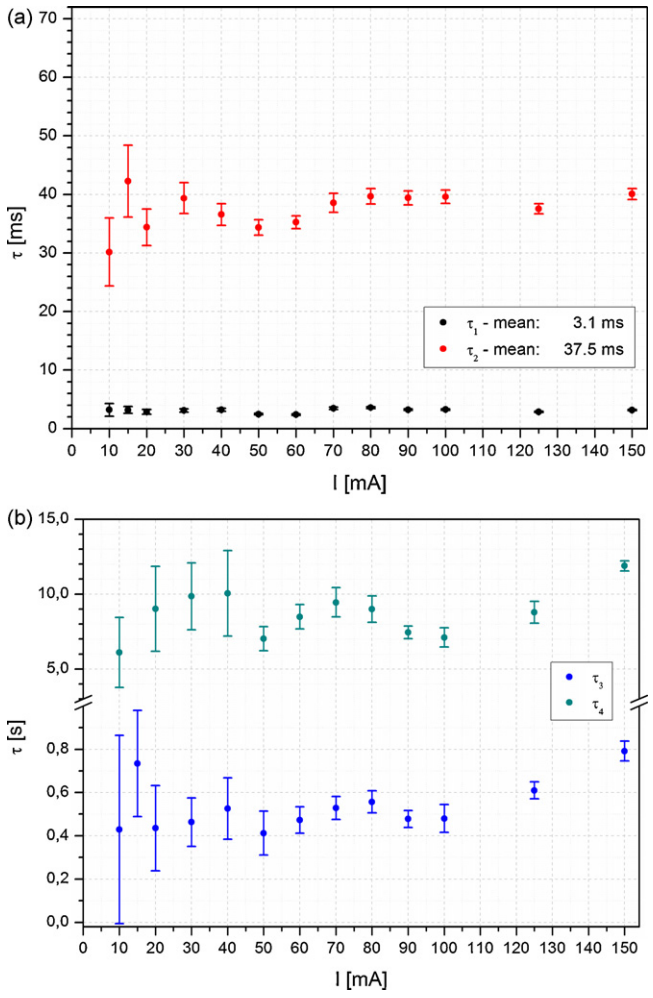

Fig. 8. Measured time constants for pulsed scan, pulsed currents from 10 mA to 150 mA, DC = 0.2: (a) current interrupt within pulse sequence and (b) current interrupt after pulse sequence.

adjust the load current to the programmed current until the end of a pulse and thus that it is valid for calculating the resistances. Little differences in the load current have a bigger impact on the calculated resistances and the actual current might be bigger than assumed (being at the lower end of the load range) and leading

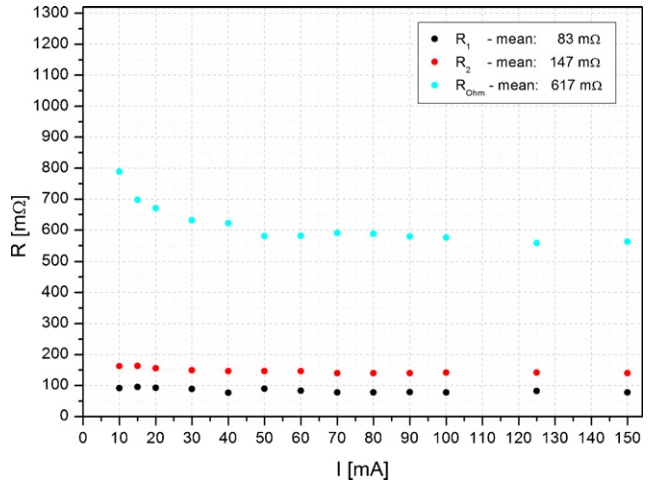

Fig. 9. Equivalent circuit resistances from current interrupt within pulse sequence, pulsed currents from 10 mA to 150 mA, DC = 0.2.

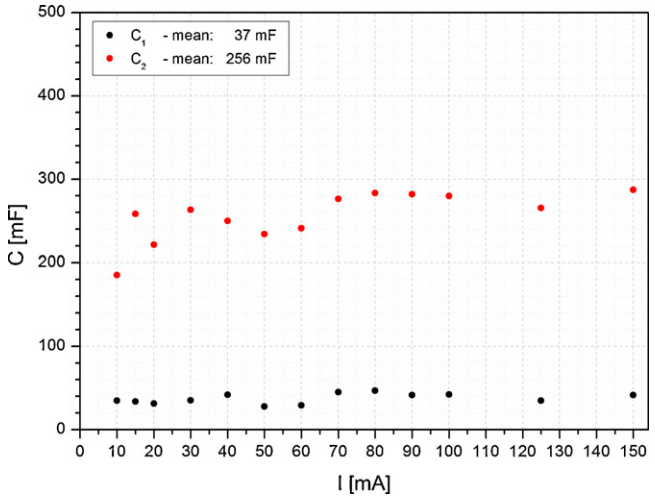

Fig. 10. Equivalent circuit capacitance from current interrupt within pulse sequence, pulsed currents from 10 mA to 150 mA, DC = 0.2.

to a higher calculated resistance. The impact of a bigger load current might result in higher calculated resistances R_1 and R_2 at the lower end of the current range as well. One should be able to see the impact of the activation overvoltage here, which should lead to smaller resistances. In general however the calculated resistances show a small variation being independent of the load current. The ohmic resistance dominates over the resistances in the dynamic elements for all load currents.

Fig. 10 illustrates the calculated capacitances. In contrast to the results of the long-term experiments the capacitances do not show such a great variation. With mean values of 37 mF for C_1 and 256 mF for C_2 both agree fairly well with the capacitances measured at the beginning of the long-term experiments.

5. Conclusion

A Zn-based gas evolving cell was studied in this paper. Considering the highly dynamic requirements posed by portable applications the dynamic characteristics of the GEC are studied experimentally. Long-term experiments are conducted to analyze the performance under continuous and pulsed load currents. A maximum hydrogen volume of 956 ml was measured for a pulsed load current of 30 mA (DC = 0.2) with an electrical energy density of 233 Wh l^{-1} and 73 Wh kg^{-1} at a cell volume of 3 cm^3 and weight of 9.58 g, respectively. Considering the generated hydrogen an energy density of 287 Wh kg^{-1} could be achieved in connection with a fuel cell. The dynamic behavior of the GEC was monitored during discharge. Time constants with a magnitude of 3 ms and 40 ms are derived from the measured voltage characteristics. These are assigned to the dynamic behavior of the electrochemical double layer at the cathode and the anode and equivalent circuit elements are calculated. The resulting resistances show a behavior increasing to a higher level after 70% of the discharge time which is similar to observed voltage characteristics, which show a significant decrease at this time. This behavior is explained by a change of the bulk conductivity within the cell. The resulting equivalent capacitances are decreasing with increasing discharge time, which also is attributed to a change in the composition of the anode. Further experiments with different load currents show a similar behavior. Additional time constants in the order of 500 ms and 10 s are observed, which are related to diffusion processes.

Variations in the measurement results can be attributed to the imprecise approach of the current interrupt technique but also to

the measurement equipment operating close to specification limits. A future characterization using electro impedance spectroscopy might yield more accurate results and could include a more detailed classification of the observed behavior, by using additional circuit elements like a Nernstian element or Warburg impedance. Due to missing material data a specific assignment of the observed processes cannot be final at this point.

Acknowledgements

This work has been supported by the Integrated Graduate Program on Human-Centric Communication at Technical University Berlin. Furthermore the authors would like to thank VARTA Microbattery GmbH for supplying the samples for the study.

References

[1] R. Hahn, S. Wagner, T. Stolle, K. Marquardt, H. Reichl, International Symposium on PowerMEMS, Tokyo, Japan, November 28–30, 2005.
[2] R. Hahn, S. Wagner, S. Krumbholz, H. Reichl, DTIP of MEMS & MOEMS, Nice, France, April 9–11, 2008.
[3] S. Wagner, S. Krumbholz, R. Hahn, H. Reichl, J. Power Sources 190 (2009) 76–82.
[4] S. Wagner, Entwicklung von Mikro-Polymermembranbrennstoffzellen unter Einsatz von Mikrostrukturierungstechnologien, Ph.D. Thesis, TU-Berlin, 2009.
[5] J. Larminie, A. Dicks, Fuel Cell Systems Explained, 2nd ed., Wiley & Sons, Chichester, 2003.
[6] D. Linden, Handbook of Batteries, 3rd ed., McGraw-Hill, 2001.
[7] G. Pistoia, Battery Operated Devices and Systems: From Portable Electronics to Industrial Products, Elsevier, New York, 2008.
[8] I.J. Ong, J. Newman, J. Electrochem. Soc. 146 (1999) 4360–4365.
[9] Y. Wang, C.-Y. Wang, Electrochim. Acta 50 (2005) 1307–1315.
[10] P. Atkins, J. de Paula, Atkins' Physical Chemistry, 8th ed., Oxford University Press, 2006.
[11] W. de Blok, J. Fortuin, D. Vermeulen, Heat Mass Transfer 17 (1982) 11–16.